HIGH-QUALITY OCTA-LEVEL FRINGE PATTERN GENERATION FOR IMPROVING THE NOISE CHARACTERISTICS OF MEASURED DEPTH MAPS

Zi-Xin XU, Yuk-Hee CHAN and Daniel P.K. LUN

Center for Multimedia Signal Processing
Dept. of Electronic and Information Engineering
The Hong Kong Polytechnic University
Email: ben.x.xu@connect.polyu.hk, enyhchan@polyu.edu.hk, enpklun@polyu.edu.hk

Abstract

Since the introduction of the binary defocusing technique, various algorithms have been proposed to optimize binary fringe patterns for reducing the phase root mean square (rms) error. Our recent study showed that octa-level fringe patterns can further reduce the phase rms error at no extra cost and patch-based fringe patterns can cause harmonic distortion to the measured depth map. This paper presents a novel method to produce patch-based octa-level fringe patterns of ideal noise characteristics by (1) formulating the optimization problem in a better way, (2) starting the optimization process with a better initial estimate and (3) adopting a necessity-oriented strategy to refine the fringe patterns during the optimization process.

1. Introduction

Non-contact three-dimensional (3D) surface sensing has been extensively studied recently [1]. Among various 3D surface measurement techniques, digital fringe projection [2] has been considered as one of the most reliable and convenient ones. A number of different fringe patterns have been developed in the literature for supporting digital fringe projection. Among them, phase-shifting sinusoidal patterns [2] are popular because they can provide high resolution and accuracy. However, as more than one fringe patterns are required to project onto the object sequentially during the measurement, it is difficult to measure a moving object.

Nowadays, the frame rate of a high-speed camera (in order of kHz) can be much higher than the frame rate of most digital light processing (DLP) projectors (typically ≤120 Hz). In view of this, methods based on binary defocusing technique [3-18] were proposed to break the speed bottleneck of a DLP projector by making use of the facts that a proper defocused binary pattern can be a good approximation of a sinusoidal pattern and that the frame rate of binary pattern projection is high enough to support real-time 3D measurement. An advantageous side effect of using binary patterns is that they are not affected by the luminance nonlinearity of a projector, which significantly improves the measuring performance.

The first suggested binary patterns are simple square binary fringe patterns (SBM) [3,4]. Various methods were then proposed to develop binary fringe patterns of better noise characteristics. The simplest approach is to redistribute the noise in a binary fringe pattern with one-dimensional (1D) pulse width modulation (PWM). Examples of these methods include SPWM [5], OPWM [6] and tripolar SPWM [7]. In [8,9], focus was put on the manipulation of the 3rd harmonic of a PWM signal in intensity domain. A comparison study on SBM, SPWM and OPWM was reported in [10]. Afterwards, researchers applied frequency modulated halftoning techniques[11] to carry out two-dimensional (2D) noise shaping [12-18]. Since the measuring performance is actually determined by the phase error achieved by the projected fringed patterns instead of the approximation error between the defocused binary patterns and their target sinusoidal patterns, there are proposals that optimize

binary patterns to minimize phase root mean square (rms) error directly [13]. However, though phase-based optimization [13] can minimize phase rms error, intensity-based optimization [14-18] can provide fringe patterns that are more robust to defocusing extent.

The idea of binary defocusing was further extended in [19,20]. The octa-level fringe patterns proposed in [19,20] can achieve all advantages of bi-level fringe patterns. By increasing the intensity levels of fringe patterns, their achieved phase rms error can be reduced sharply. To reduce the optimization effort and introduce flexibility, current fringe pattern generation methods[16-20] generally optimize patches and construct fringe patterns by tiling the optimized patches. The tiling output is a regular periodic pattern and hence the measured depth map of an object can contain serious harmonic distortion. The proposal in [20] takes this issue into account and reduces the harmonic distortion along a specific direction significantly. However, harmonic distortion can still be found in the other orthogonal direction.

Though conventional fringe pattern generation methods formulate the pattern generation as an optimization problem, the problem is generally solved by iteratively refining an initial estimate due to its unaffordable complexity. The solution is generally not the global optimum but a local optimum in terms of an objective function. When the refining step is not flexible, the solution can be biased to the initial estimate and its performance can be far from the optimal. In view of this, a better initial estimate and a flexible refining scheme would definitely be helpful to get better fringe patterns.

This paper proposes a novel method to generate patch-based octa-level fringe patterns for improving the measuring performance of a 3D surface measuring system. As compared with the state-of-art patch-based octa-level fringe pattern generation method [20], its contributions include:

(1) A new method is proposed to optimize patches such that they can be flexibly and seamlessly tiled to form octa-level fringe patterns the achieved phase error of which contains almost no harmonic distortion along any direction.

(2) A new approach is proposed to get a better initial estimate of the fringe patterns for further refinement such that fringe patterns of better noise characteristics can be obtained after the optimization process.

(3) A more flexible and efficient approach is proposed to refine the fringe patterns such that the optimization process can converge faster to a solution of better noise characteristics.

The remainder of this paper is organized as follows. In Section 2, we briefly review the working principle of a three-step phase-shifting algorithm. The ideas of binary defocusing and octa-level fringe pattern projection are also reviewed. Section 3 introduces the proposed new approach for optimizing octa-level patch-based fringe patterns. Sections 4 and 5 respectively present the simulation and the experimental results for performance evaluation. Finally, a conclusion is provided in Section 5.

2. A background review

Phase-shifting algorithms have been extensively used in 3D surface measurement because it can provide high accuracy and robustness. A simple three-step phase-shifting algorithm projects three sinusoidal fringe patterns, each of which has a phase shift of $2\pi/3$ from each other, onto the surface of the object to be measured. Accordingly, three phase-shifted fringe images, denoted as I_k for $k \in \{1,2,3\}$, can be captured with a high speed camera. Their intensity values at pixel (x, y) are given as:

$$I_1(x,y) = A(x,y) + M(x,y)cos(\varphi(x,y) - 2\pi/3) \quad (1)$$

$$I_2(x,y) = A(x,y) + M(x,y)cos\big(\varphi(x,y)\big) \quad (2)$$

$$I_3(x,y) = A(x,y) + M(x,y)cos(\varphi(x,y) + 2\pi/3) \quad (3)$$

where $A(x,y)$ is the average intensity, $M(x,y)$ denotes the amplitude of intensity modulation, and $\varphi(x,y)$ symbolizes the pixel-wise phase to be solved. By solving the three equations, a pixel-wise phase map can be obtained as:

$$\varphi(x,y) = \tan^{-1}(\sqrt{3}\frac{I_1(x,y)-I_3(x,y)}{2I_2(x,y)-I_1(x,y)-I_3(x,y)}) \quad (4)$$

$\varphi(x,y)$ is a wrapped phase ranging in [-π, π]. After unwrapping $\varphi(x,y)$, the depth information of the object can be obtained[21].

To speed up the measurement process, 8-bit sinusoidal patterns can be replaced with binary patterns such that the frame rate is only limited by the switching rate of the projection [4]. The binary patterns are designed in a way that, after being defocused by the projector, they can well approximate the sinusoidal patterns.

Without sacrificing the speed and other advantages of binary defocusing methods, Xu and Chan suggested using octa-level patterns to replace binary patterns such that the approximation error can be further reduced[19,20]. In consequence, the accuracy of $\varphi(x,y)$ can be improved. The proposal is based on the fact that the red (R), green (G) and blue (B) color channels of a projector are handled independently. Accordingly, one can define binary patterns B_R, B_G and B_B for channels R, G and B respectively to compose a color fringe image whose luminance component is an octa-level pattern generally determined as

$$L = 0.299B_R + 0.587B_G + 0.114B_B \quad (5)$$

When we project the color fringe image onto the object and then extract the luminance plane of the color image captured by the camera, it is equivalent to projecting an octa-level fringe pattern onto the object directly. Since the octa-level patterns are actually produced by manipulating binary patterns in individual channels, the advantages of binary defocusing can be maintained while the measurement performance is improved. As compared with binary fringe patterns, the only disadvantage of octa-level fringe patterns is that more preparation effort is required to develop the patterns since it involves the manipulation of three binary planes. However, fringe pattern development is a one-time process. In practice there is no extra cost for subsequent measurements once the fringe patterns are developed.

3. Proposed octa-level fringe pattern generation method

3.1 Generation of initial fringe patterns

Conventional binary defocusing methods[13-18] first generate initial binary fringe patterns and then refine them to produce the final binary fringe patterns for approximating sinusoidal patterns. This two-stage process is also adopted in [19,20] to develop octa-level fringe patterns. To follow the tradition, conventional error diffusion (CED) [22] is exploited in [20] to generate initial octa-level fringe patterns with an octa-level quantizer. CED diffuses the quantization error to a pre-defined direction with a fixed causal diffusion filter and hence causes directional hysteresis[23,24].

The subsequent refinement step cannot guarantee a globally optimized approximation result. It implies that the approximation performance of the final octa-level fringe patterns is initial-estimate dependent. In general, we can expect that a better initial estimate can lead to a better final fringe pattern. In view of this, a modified version of feature-preserving multiscale error diffusion (FMED) is adopted here to generate our initial octa-level patterns as FMED has already been proven to be good at producing binary and multi-level halftoning results that possess ideal noise characteristics [25-27].

Let S_k for $k\in\{1,2,3\}$ be three sinusoidal fringe patterns and L_k be the corresponding octa-level fringe pattern that approximates S_k. Without loss of generality, we assume that S_k is scaled and offsetted such that its minimum and maximum are, respectively, 0 and 1. Fringe patterns L_k for $k\in\{1,2,3\}$ are generated separately. For each k, an error image E_k is initialized to be S_k at the

beginning. Pixels of L_k are then picked iteratively to determine their intensity values until all pixel values of L_k are determined. The steps in each iteration cycle are as follows:

1) Select a pixel in L_k via the extreme error intensity guidance (EEIG) based on the most updated E_k. One may refer to [23,24] for the details of EEIG. Let the selected pixel position be (m,n).
2) Quantize $E_k(m,n)$ to the nearest value in $\Psi=\{0.299r+0.587g+0.114b|r,g,b\in\{0,1\}\}$ and assign the quantized value to $L_k(m,n)$.
3) Update E_k by diffusing the quantization error, which is $Q(m,n)=E_k(m,n)-L_k(m,n)$, to the neighborhood of $E_k(m,n)$ with an adaptive non-causal diffusion filter as follows.

$$E_k(i,j)=\begin{cases}0 & \text{if } (i,j)=(m,n)\\ E_k(i,j)+\frac{f(i-m,j-n)\cdot D(i,j)\cdot Q(m,n)}{K} & \text{if } (i-m,j-n)\in\Omega\end{cases} \quad (6)$$

$$\text{where } f(p,q)=\begin{cases}0.0717 & \text{if } |p|=|q|=1\\ 0 & \text{if } p=q=0\\ 0.1783 & \text{if } |p|+|q|=1\end{cases} \quad (7)$$

is a filter coefficient of a non-causal filter whose support is $\Omega=\{(p,q)|p,q\in\{-1,0,1\}\}$,

$$D(i,j)=\begin{cases}0 & \text{if } L_k(i,j)\text{'s value has been determined}\\ 1 & \text{else}\end{cases}, \quad (8)$$

and

$$K=\sum_{(i-m,j-n)\in\Omega}\big(f(i-m,j-n)\cdot D(i,j)\big) \quad (9)$$

When K=0, a filter with a larger support window is exploited as suggested in [25] to allow the algorithm to proceed.

Figs. 1(a) and (b) show two octa-level fringe patterns and their corresponding noise spectra. They were respectively produced with the CED-based approach used in [20] and the proposed FMED-based approach to approximate a sinusoidal fringe pattern whose period is 60 pixels. From their corresponding noise spectra, one can see that the former carries serious harmonic distortion while the latter does not. Besides, most of the noise in the fringe pattern shown in Fig. 1(b) is high frequency noise, which can actually be removed by the defocusing process when the fringe pattern is projected onto an object during measurement. In fact, by modeling the defocusing process as a 5×5 Gaussian filtering process as in [13-20], the rms errors of the defocusing outputs of the fringe patterns shown in Figs. 1(a) and (b) are, respectively, 0.0115 and 0.0077 with respect to the grayscale sinusoidal pattern. The octa-level fringe pattern produced with the proposed FMED-based approach is obviously better.

If we do not opt for patch-based octa-level fringe patterns, we can directly use L_k for $k\in\{1,2,3\}$ as the initial estimate to start an iterative optimization process. However, since we aim for patch-based fringe patterns, we extract patches from L_k to construct patch-based initial fringe patterns for optimizing the patches. The details will be discussed in the following sections.

3.2 Formulation of the optimization problem

To allow flexibility in practical applications, two sets of three octa-level patches are optimized in [20] such that octa-level fringe patterns of any desirable sizes can be flexibly and easily constructed by tiling the optimized patches on site whenever necessary. Patch tiling tends to produce regular and periodic patterns that introduce harmonic distortion. To solve this problem, special care is taken during the optimization in [20] to make sure that a tiling output is aperiodic along a specific direction. In this paper, we extend the idea to further improve the optimization objective function such that both horizontal and vertical periodicity can be avoided when tiling the optimized octa-level patches.

Let $P_{(s,k)}$ be the k^{th} octa-level patch of set $s\in\{0,1\}$, where $k\in\{1,2,3\}$. Each patch is of size $N_y \times N_x$, where N_x is the period of the target sinusoidal patterns and N_y is an integer value. In our approach, for each k, we tile patches $P_{(1,k)}$ and $P_{(2,k)}$ as shown in Figure 2 to form an octa-level pattern P_k and then optimize P_k for $k\in\{1,2,3\}$ simultaneously to minimize an objective function. Note that in pattern P_k the occurrences of all possible horizontal and vertical connection combinations between any two patches randomly and independently picked from $\{P_{(s,k)}|\ s=0,1\}$ are identical. There is no bias to favor a particular connection combination during the optimization, which guarantees that they can be seamlessly connected to each other when they are tiled horizontally and vertically.

To make the approximation performance robust to amount of defocusing, the objective function to be minimized in the optimization is selected as

$$J = \Delta\varphi^5 + \Delta\varphi^{11} \tag{10}$$

where $\Delta\varphi^t$ for $t=\{5,11\}$ denotes the phase root mean square (rms) error achieved when the amount of defocusing can be modeled as the filtering effect of a $t\times t$ Gaussian filter with standard deviation equal to $t/3$(denoted as G_t afterwards)[13-20]. In formulation, $\Delta\varphi^t$ is defined as:

$$\Delta\varphi^t = \sqrt{\sum_{x=0}^{M-1}\sum_{y=0}^{N-1}(\varphi(x,y) - \varphi_{G_t}(x,y))^2/MN} \tag{11}$$

where $N \times M = 8N_y \times 8N_x$ is the size of P_k and φ_{G_t} is the phase map obtained when the sinusoidal fringe patterns are replaced with the octa-level fringe patterns defocused by filter G_t.

In summary, our optimization problem to be solved is formulated as

$$\min_{P_{(s,k)} \text{ for } s\in\{1,2\},k\in\{1,2,3\}} J \tag{12}$$

subject to the constraints that P_k is constructed with $P_{(s,k)}$ for $s=1,2$ as shown in Figure 2 and that

$$P_{(s,k)} = 0.299B_{R_{(s,k)}} + 0.587B_{G_{(s,k)}} + 0.114B_{B_{(s,k)}} \tag{13}$$

where $B_{R_{(s,k)}}$, $B_{G_{(s,k)}}$ and $B_{B_{(s,k)}}$ are three $N_y\times N_x$ binary patterns representing the intensity variations in color channels R, G and B respectively.

3.3 Fast convergence optimization

The optimization problem formulated in Section 3.2 is a NP hard problem. When solving an optimization problem to develop a binary fringe pattern, conventional binary defocusing algorithms [13-20] generate an initial estimate of the pattern and then refine it iteratively to get a sub-optimal solution. In each iteration cycle, pixels in a fringe pattern are adjusted one by one[13-16,18-20] or group by group [17] according to a fixed raster scanning order. The adjustment is realized by replacing the current pixel value with the 'best' value that is determined through an exhaustive search among all possible pixel values. This process is very time-consuming and the non-flexible static scanning order adopted in each refinement iteration cycle makes the final solution easily trapped in a sub-optimal local minimum that is very close to the initial estimate. Though the complexity issue can be alleviated a bit when the fringe patterns are patch-based[16-20], the trapping issue can be very problematic.

In this paper, we propose to adjust pixels according to a necessity-oriented order instead of a location-oriented order. The introduced flexibility and adaptivity make the optimization converge much faster and avoid being trapped in a local optimum before exploring sufficient possibilities. This optimization algorithm is referred to as necessity oriented optimization(NOO) and its details are as follows:

Step 1. Initialization of $P_{(s,k)}$ for $s\in\{1,2\}$:

Generate three octa-level patterns L_k for $k\in\{1,2,3\}$ to approximate three sinusoidal fringe patterns with the FMED-based technique presented in Section 3.1. Chop two connected $N_y\times N_x$ segments from each of them to form initial patches $P_{(s,k)}$ for $s\in\{1,2\}$. P_k is then constructed with $P_{(1,k)}$ and $P_{(2,k)}$ as shown in Figure 2.

Step 2. Refining $P_{(s,k)}$ for $s\in\{1,2\}$ based on a necessity-oriented strategy:

As shown in Fig. 2, P_k can be partitioned into 64 blocks of size $N_y\times N_x$ and each of them is either patch $P_{(1,k)}$ or $P_{(2,k)}$. Accordingly, these blocks are divided into two groups based on the criterion whether they are $P_{(1,k)}$ or $P_{(2,k)}$. Once a pixel in a patch is adjusted, all the blocks in the same corresponding group will be affected. Let $P_{k(m,n)}$ be the (m,n)th block of P_k for $0\le m,n<8$ and $P_{k(m,n)}(p,q)\equiv P_k\left(mN_x+p,nN_y+q\right)$ be the (p,q)th pixel in block $P_{k(m,n)}$. In formulation, the grouping can be done based on the index of a block and it is given as

$$\Lambda_s=\{(m,n)|0\le m,n<8 \text{ and } P_{k(m,n)}\ is\ P_{(s,k)}\}\quad \text{for } s\in\{1,2\}. \tag{14}$$

For a specific patch combination, the contribution of the (i,j)th pixels of patches $P_{(s,1)}$, $P_{(s,2)}$ and $P_{(s,3)}$ to absolute phase error ε is roughly given as

$$\varepsilon(i,j;s)=\sum_{(m,n)\in\Lambda_s}\sum_{t=5,11}\left|\varphi\left(mN_x+i,nN_y+j\right)-\varphi_{G_t}(mN_x+i,nN_y+j)\right| \tag{15}$$

We sort triplets in set $T=\{(i,j;s)|0\le i<N_x,0\le j<N_y \text{ and } s\in\{1,2\}\}$ according to the value of $\varepsilon(i,j;s)$ in descending order and then pick the triplets from the sorted triplet sequence one by one. When triplet $(i,j;s)$ is picked, the (i,j)th pixels of patches $P_{(s,k)}$ for k=1,2,3 are adjusted simultaneously. The picking stops when $\varepsilon(i,j;s)<\varepsilon(i_o,j_o;s_o)/10$, where $(i_o,j_o;s_o)$ is the first triplet in the sorted sequence.

Assume that the currently picked triplet is $(i',j';s')$. Since $P_{(s',k)}(i',j')$ is an octa-level value, there are altogether 8^3=512 possible value combinations of $P_{(s',k)}(i',j')$ for $k\in\{1,2,3\}$. For each combination, construct a candidate set of patches $P_{(s',1)}$, $P_{(s',2)}$ and $P_{(s',3)}$ (denoted as $P^c_{(s',1)}$, $P^c_{(s',2)}$ and $P^c_{(s',3)}$ respectively) in which we have $P^c_{(s',k)}(i,j)=P_{(s',k)}(i,j)$ for all $(i,j)\neq(i',j')$, and update fringe patterns P_k for all k by replacing blocks $P_{k(m,n)}$ with $P^c_{(s',k)}$ for $(m,n)\in\Lambda_{s'}$. Among all 512 candidate sets of patches, the one used to construct the fringe patterns that minimize J is selected to be the most updated $P_{(s',1)}$, $P_{(s',2)}$ and $P_{(s',3)}$.

Step 3. Termination analysis:

If the total improvement in step 2 is larger than 0.01% in terms of J, go back to step 2. Otherwise the most updated $P_{(1,k)}$ and $P_{(2,k)}$ for $k\in\{1,2,3\}$ are considered as the optimal patches.

Step 4. Finalizing fringe patterns:

Randomly tile optimized patches $P_{(1,k)}$ and $P_{(2,k)}$ horizontally and vertically to form full-size octa-level fringe patterns L'_k for $k\in\{1,2,3\}$ under the condition that L'_1, L'_2 and L'_3 share the same random tiling pattern. This step can be done on site to cater for different systems.

4. Simulations

Simulations were carried out to evaluate the performance of the proposed octa-level fringe patterns (referred to as *cpatch2D* hereafter.). The performance was measured in terms of the phase error achieved with the defocused fringe patterns. For comparison, the fringe patterns proposed in [16], [19] and [20] (referred to as *bpatch*, *cpatch* and *cpatch1D* respectively hereafter) were also evaluated. All fringe patterns were patch-based patterns and optimized to handle a specific defocusing condition as described in their original designs. In our simulations, the defocusing process of a projector was modeled as a 5×5 Gaussian filter with its standard derivation equal to 5/3 unless else specified. The horizontal (i.e. x-) dimension of a fringe pattern corresponds to the direction of the sinusoidal variation in the target sinusoidal fringe pattern that it approximates.

The first simulation was for investigating whether the proposed method could effectively eliminate harmonic distortion in its produced octa-level fringe patterns. In the simulation, all fringe patterns were of size 1024×768 pixels and the fringe period of the target sinusoidal fringe patterns to be approximated was 60 pixels.

Fig. 3 shows the normalized amplitude noise spectra of the phase maps achieved by *bpatch*, *cpatch*, *cpatch1D* and *cpatch2D* under the specified defocusing condition. The magnitudes of the components in all 4 plots are normalized with respect to the strongest component in all 4 plots for easier comparison. The advantage of the proposed patterns is obvious in the plots. The outstanding regular peaks in the plot of *bpatch* reflect that there are strong harmonic components in its phase error. The situation is gradually improved by *cpatch* and *cpatch1D*. *cpatch1D* can only handle the horizontal periodicity in a tiled fringe pattern, so there are still vertical harmonic components. In contrast, the harmonic distortion in both directions is almost eliminated in the phase map achieved by *cpatch2D*.

Fig. 4 shows a cross-section of an ideal sinusoidal fringe pattern along the x-direction and the corresponding cross sections of the defocused patterns of *cpatch1D* and *cpatch2D*. Only *cpatch1D* and *cpatch2D* are compared here as *bpatch* and *cpatch* are not designed to handle the harmonic distortion of a tiled fringe pattern. One can see that the proposed fringe pattern is closer to the ideal sinusoidal signal after defocusing. This superiority is achieved with the proposed necessity oriented optimization scheme and the better initial patterns used in the optimization scheme. Note that both *cpatch1D* and *cpatch2D* attempt to minimize the phase error achieved by the fringe patterns instead of the approximation error between an octa-level fringe pattern and the target sinusoidal fringe pattern. Theoretically, when phase-domain optimization is adopted, the resultant fringe patterns are not necessary to be ideally sinusoidal as long as the phase error is minimized under a specific defocusing condition [15]. However, the lower the approximation error, the more robust to the defocusing extent the measuring performance is. This advantage helps *cpatch2D* to perform better in real experiments when the defocusing condition cannot be controlled perfectly.

Fig. 5 shows some simulation data for measuring a complex three-dimensional surface. In the simulation, the fringe periods of all fringe patterns were 60 pixels, and a simple phase unwrapping algorithm (Goldstein et al.'s branch cut method [21]) was exploited. The defocusing process was modeled as a 5×5 Gaussian filter with standard derivation equal to 5/3. We can observe that the object is flooded in the noise in *bpatch*'s result. The harmonic distortion in *cpatch*'s and *cpatch1D*'s results provides misleading messages as a set of false parallel ridges are mixed with the true ones. In contrast, the object surface can be reported more faithfully in our result. As a matter of fact, the corresponding phase rms errors of Figs. 5(c), (d), (e) and (f) are, respectively, 0.0221, 0.0089, 0.0048 and 0.0042 (in rad).

The proposed necessity-oriented patch-based fringe pattern optimization scheme can also speed up the optimization process besides improving its optimization result. Fig. 6 shows the difference in convergence speed when adopting the raster-scanned ordering used in [20] instead of the necessity-oriented ordering in step 2 of NOO. Each curve in the plot shows how the value of the objective

function defined in eqn.(10) decreases with number of iterations in our simulation. The fringe period is 60 pixels and the patch size is 20×60 pixels. The convergence speed is much faster when the necessity-oriented ordering is used.

5. Experiments

A real 3D shape measurement system was set up to verify the performance of the proposed technique. The system consists of a DLP projector (Texas MP723) and a charge-coupled-device (CCD) camera (Canon 400D). The size of a projected fringe pattern is 1024×768 pixels. In the first experiment we measured a flat black board placed around 0.5 meters away from the projector.

The ground truth is obtained by measuring the object with the grayscale nine-step phase-shifting algorithm [2]. To tackle the gamma nonlinearity of the projector, active gamma correction [28] was done to produce the grayscale sinusoidal fringe patterns. When binary or octa-level fringe patterns were applied, the projector was adjusted to different defocusing levels to verify their robustness to defocusing. The phase rms errors achieved by different defocused bi/octa-level patterns are illustrated in Fig. 7.

It is found that the phase rms errors of octa-level fringe patterns (*cpatch*, *cpatch1D* and *cpatch2D*) are smaller than binary patterns (*bpatch*) due to the increase of gray levels. When the projector is slightly defocused, the performance of *cpatch1D* and *cpatch2D* is similar. However, when the projector is more defocused, *cpatch2D* outperforms *cpatch1D*. *cpatch2D* is more robust to defocusing.

In another experiment, a jug shown in Fig. 8(a) was placed around 50cm away from the projector and measured by projecting different fringe patterns. The fringe periods of all tested fringe patterns were 18 pixels. Figs. 8(b)-(e) show the luminance channels of the images captured with the camera when different fringe patterns were projected onto the object.

Fig. 9(a) shows the jug's depth map (unit in cm) obtained with the grayscale nine-step phase-shifting algorithm [2]. Active gamma correction [28] was carried out to reduce the gamma nonlinearity of the projector and a simple phase unwrapping algorithm [21] was applied to get the absolute phase. The obtained depth map was used as the reference for comparison. Figs. 9(b), (c), (d) and (e) show, respectively, the depth maps obtained with *bpatch, cpatch*, *cpatch1D* and *cpatch2D*. Their corresponding depth rms error are, respectively, 0.1133, 0.0671, 0.0583 and 0.0240 cm. Note that no gamma calibration for the projector is required when these fringe patterns were used.

6. Conclusions

In this paper, we propose a framework to generate high quality octa-level fringe patterns for real time 3D shape measurement. By adopting better approaches to formulate the optimization problem, produce initial fringe pattern estimates for optimization and refine the fringe patterns during the optimization process, the developed fringe patterns can achieve a better measuring performance. Specifically, the phase map produced with the optimized fringe patterns contains almost no harmonic distortion along any direction and little low frequency noise. Though the optimization is carried out in the phase domain, the generated fringe patterns are close to ideal sinusoidal patterns after being defocused, which makes them robust to defocusing extent in real world situations. Moreover, the optimization process is much faster than the one used in the state-of-art octa-level fringe pattern generation algorithm[20].

Acknowledgments

This work was supported by Multimedia Signal Processing Center and The Hong Kong Polytechnic University under Grant number G-YBM9.

References

[1] Gorthi S, Rastogi P. Fringe projection techniques: whither we are? Opt Lasers Eng 2010;48:133–40.
[2] Malacara D. Optical shop testing. 3rd ed. New York: Wiley; 2007.
[3] Su X-Y, Zhou W-S, von Bally G, Vukicevic D. Automated phase-measuring profilometry using defocused projection of a Ronchi grating. Opt Commun 1992;94:561–73.
[4] Lei S, Zhang S. Flexible 3-D shape measurement using projector defocusing. Opt Lett 2009;34:3080.
[5] Ayubi G a, Ayubi J a, Di Martino JM, Ferrari J a. Pulse-width modulation in defocused three-dimensional fringe projection. Opt Lett 2010;35:3682–4.
[6] Wang Y, Zhang S. Optimal pulse width modulation for sinusoidal fringe generation with projector defocusing. Opt Lett 2010;35:4121.
[7] Zuo C, Chen Q, Feng S, Feng F, Gu G, Sui X. Optimized pulse width modulation pattern strategy for three-dimensional profilometry with projector defocusing. Appl Opt 2012;51:4477.
[8] Zuo C, Chen Q, Gu G, Ren J, Sui X, Zhang Y. Optimized three-step phase-shifting profilometry using the third harmonic injection. Opt Appl 2013;43.
[9] Zuo C, Chen Q, Gu G, Feng S, Feng F, Li R, et al. High-speed three-dimensional shape measurement for dynamic scenes using bi-frequency tripolar pulse-width-modulation fringe projection. Opt Lasers Eng 2013;51:953–60.
[10] Wang Y, Zhang S. Comparison of the squared binary, sinusoidal pulse width modulation, and optimal pulse width modulation methods for three-dimensional shape measurement with projector defocusing. Appl Opt 2012;51:861.
[11] Lau DL, Arce GR. Modern digital halftoning. 2rd ed. CRC Press; 2008.
[12] Wang Y, Zhang S. Three-dimensional shape measurement with binary dithered patterns. Appl Opt 2012;51:6631.
[13] Dai J, Zhang S. Phase-optimized dithering technique for high-quality 3D shape measurement. Opt Lasers Eng 2013;51:790–5.
[14] Lohry W, Zhang S. Genetic method to optimize binary dithering technique for high-quality fringe generation. Opt Lett 2013;38:540.
[15] Dai J, Li B, Zhang S. Intensity-optimized dithering technique for three-dimensional shape measurement with projector defocusing. Opt Lasers Eng 2014;53:79–85.
[16] Dai J, Li B, Zhang S. High-quality fringe pattern generation using binary pattern optimization through symmetry and periodicity. Opt Lasers Eng 2014;52:195–200.
[17] Sun J, Zuo C, Feng S, Yu S, Zhang Y, Chen Q. Improved intensity-optimized dithering technique for 3D shape measurement. Opt Lasers Eng 2015;66:158–64.
[18] Li X, Zhang Z, Yang C. High-quality fringe pattern generation using binary pattern optimization based on a novel objective function. Opt - Int J Light Electron Opt 2016;127:5322–7.
[19] Xu Z-X, Chan Y-H. Optimized multilevel fringe patterns for real-time 3D shape measurement with defocused projector. 2015 IEEE Int. Conf. Image Process. 2015, p. 2730–4.
[20] Xu Z-X, Chan Y-H. Removing harmonic distortion of measurements of a defocusing three-step phase-shifting digital fringe projection system., Opt Lasers Eng 2017;90:139–145.
[21] Goldstein RM, Zebker HA, Werner CL. Satellite radar interferometry: two-dimensional phase unwrapping. Radio Sci 1988; 23(4):713–720..
[22] Floyd RW, Steinberg L. Adaptive algorithm for spatial greyscale 1976;17:75–7.
[23] Chan Y-H. A modified multiscale error diffusion technique for digital halftoning. IEEE Signal Process Lett 1998;5:277–80.
[24] Chan Y-H. Feature-preserving multiscale error diffusion for digital halftoning. J Electron Imaging 2004;13:639.
[25] Fung Y-H, Chan Y-H. Optimizing the error diffusion filter for blue noise halftoning with multiscale error diffusion. IEEE Trans Image Process 2013;22:413–7.
[26] Wong L-Y and Chan Y-H. A feature preserving multilevel halftoning algorithm. J Electron Imaging 21(4), (2012).
[27] Fung Y-H, Chan Y-H. Tone-dependent noise model for high-quality halftones. J Electron Imaging 22 (2), (2013).
[28] Zhang S. Active versus passive projector nonlinear gamma compensation method for high-quality fringe pattern generation. International Society for Optics and Photonics; 2014, p.911002.

HIGH-QUALITY OCTA-LEVEL FRINGE PATTERN GENERATION FOR IMPROVING THE NOISE CHARACTERISTICS OF MEASURED DEPTH MAPS

Zi-Xin XU, Yuk-Hee CHAN and Daniel P.K. LUN

Center for Multimedia Signal Processing
Dept. of Electronic and Information Engineering
The Hong Kong Polytechnic University
Email: ben.x.xu@connect.polyu.hk, enyhchan@polyu.edu.hk, enpklun@polyu.edu.hk

List of figure Captions

Fig. 1 Preliminary octa-level fringe patterns obtained with different methods and their noise spectra: (a) CED-based [20] and (b) FMED-based. The magnitudes of all components in both spectra are normalized with respect to the strongest component in CED-based approach's spectrum for easier comparison. The color bar shown in Fig.1(c) is shared by both spectra to map magnitude values into colors.

Fig. 2 Constructing a circular connected octa-level pattern P_k with two octa-level patches for optimization

Fig. 3 Normalized noise spectra of the phase maps associated with *bpatch*, *cpatch*, *cpatch1D* and *cpatch2D*.

Fig. 4 Cross-sections of defocused fringe patterns *cpatch1D* and *cpatch2D.* The defocusing is achieved with a 5×5 Gaussian filter with a standard deviation of 5/3.

Fig. 5 Simulation results for measuring an object. (a) 3D plot of an object. (b) ideal unwrapped phase map of (a); and unwrapped phase maps obtained with (c) *bpatch*, (d) *cpatch*, (e) *cpatch1D* and (f) *cpatch2D*. The horizontal and the vertical dimensions are x- and y-dimensions respectively in (b)-(f).

Fig. 6 Impacts of different ordering schemes on convergence speed

Fig. 7 Experimental phase rms errors obtained with (a) a slightly defocused projector and (b) a more defocused projector when different bi-/octa-level fringe patterns are used.

Fig. 8 Images captured when different fringe patterns are projected onto a measured object. (a) no projection, (b) *bptach*, (c) *cpatch*, (d) *cpatch1D* and (e) *cpatch2D*.

Fig. 9 Depth maps obtained with (a) sinusoidal fringe patterns, (b) *bptach*, (c) *cpatch*, (d) *cpatch1D* and (e) *cpatch2D*.

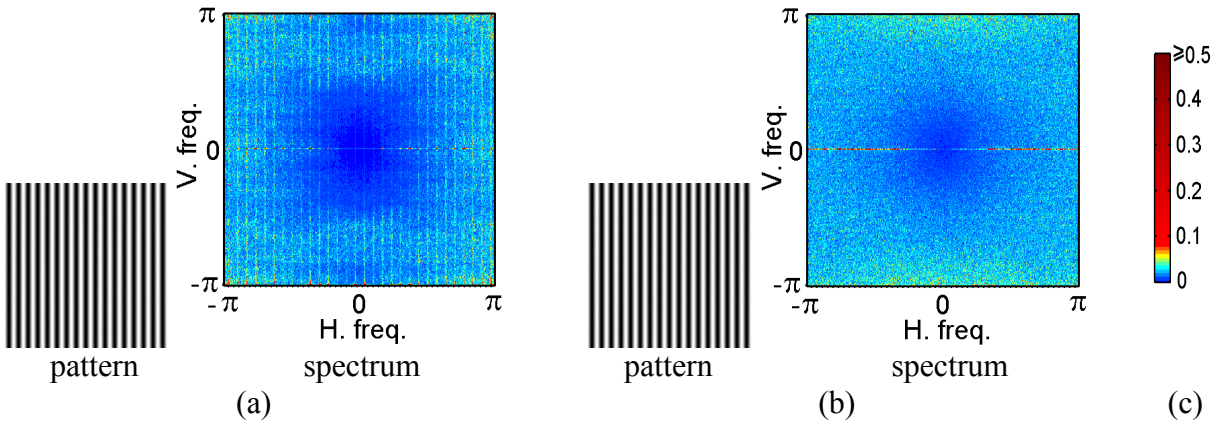

Fig. 1 Preliminary octa-level fringe patterns obtained with different methods and their noise spectra: (a) CED-based [20] and (b) FMED-based. The magnitudes of all components in both spectra are normalized with respect to the strongest component in CED-based approach's spectrum for easier comparison. The color bar shown in Fig.1(c) is shared by both spectra to map magnitude values into colors.

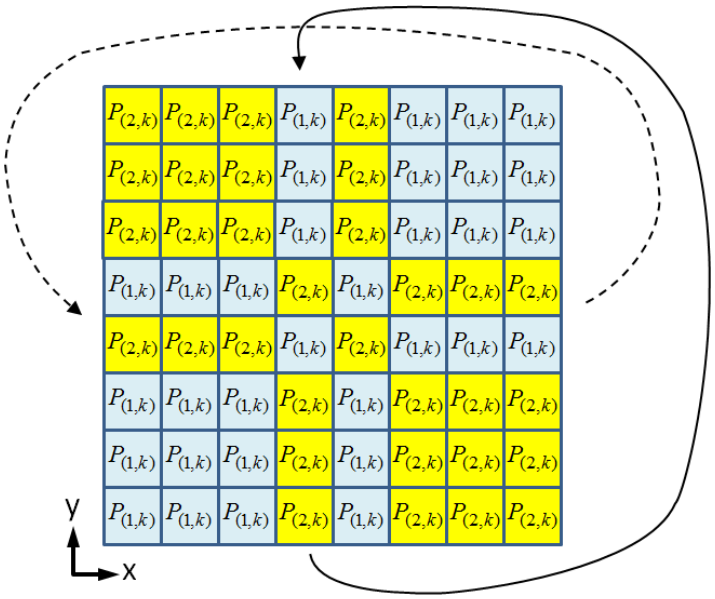

Fig. 2 Constructing a circular connected octa-level pattern P_k with two octa-level patches for optimization

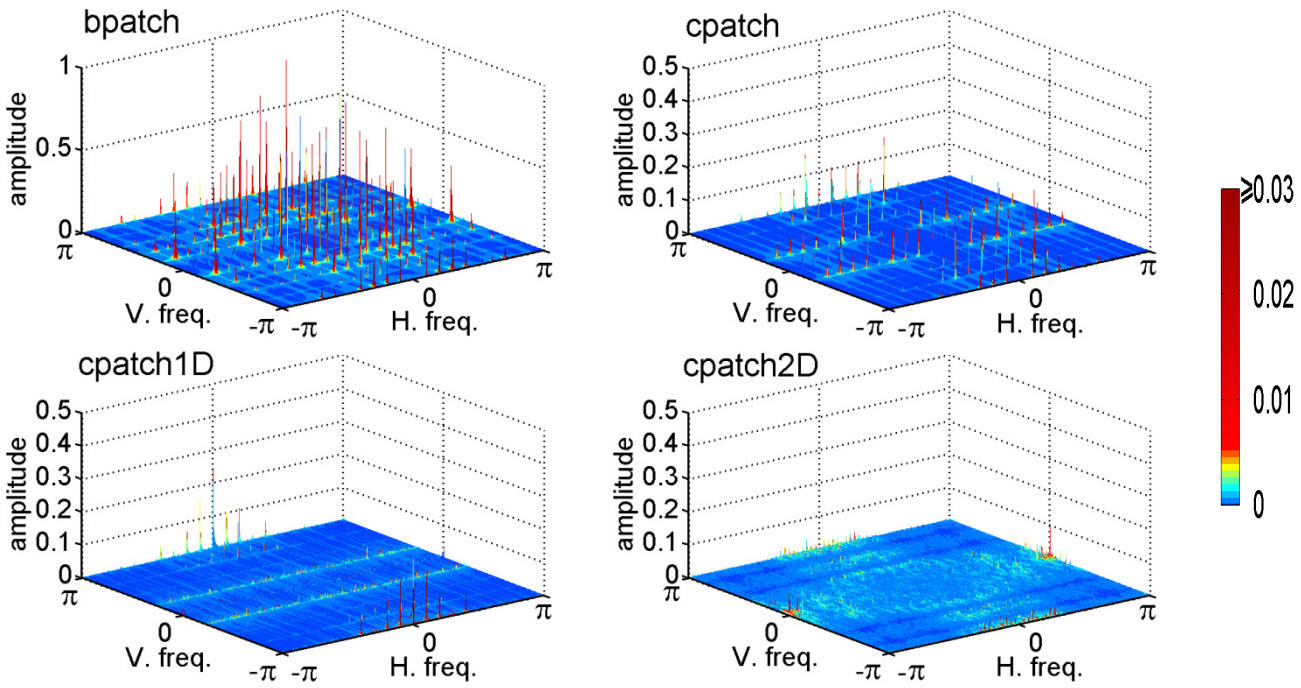

Fig. 3 Normalized noise spectra of the phase maps associated with *bpatch*, *cpatch*, *cpatch1D* and *cpatch2D*.

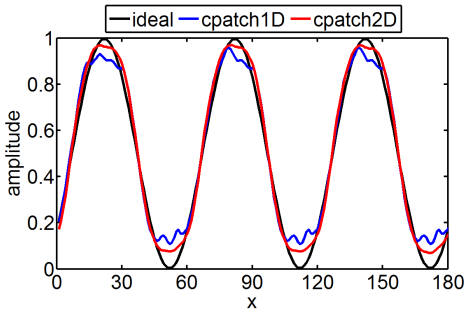

Fig. 4 Cross-sections of defocused fringe patterns *cpatch1D* and *cpatch2D*. The defocusing is achieved with a 5×5 Gaussian filter with a standard deviation of 5/3.

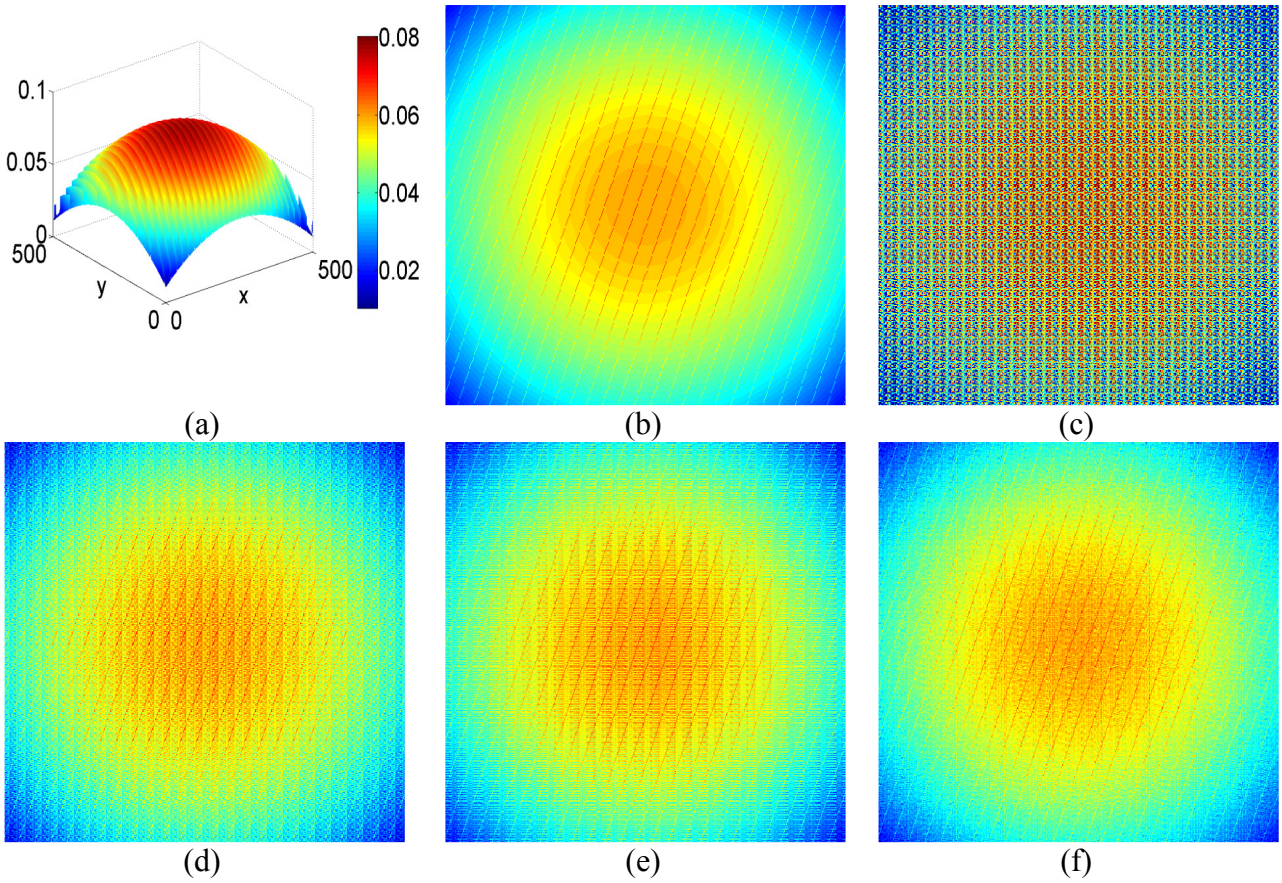

Fig. 5 Simulation results for measuring an object. (a) 3D plot of an object. (b) ideal unwrapped phase map of (a); and unwrapped phase maps obtained with (c) *bpatch*, (d) *cpatch*, (e) *cpatch1D* and (f) *cpatch2D*. The horizontal and the vertical dimensions are x- and y-dimensions respectively in (b)-(f).

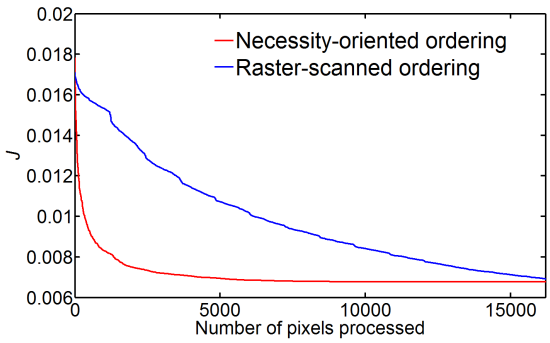

Fig. 6 Impacts of different ordering schemes on convergence speed

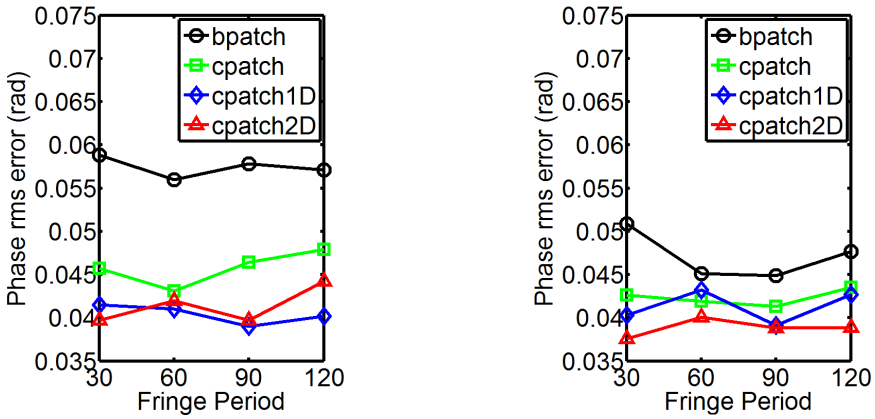

Fig. 7 Experimental phase rms errors obtained with (a) a slightly defocused projector and (b) a more defocused projector when different bi-/octa-level fringe patterns are used.

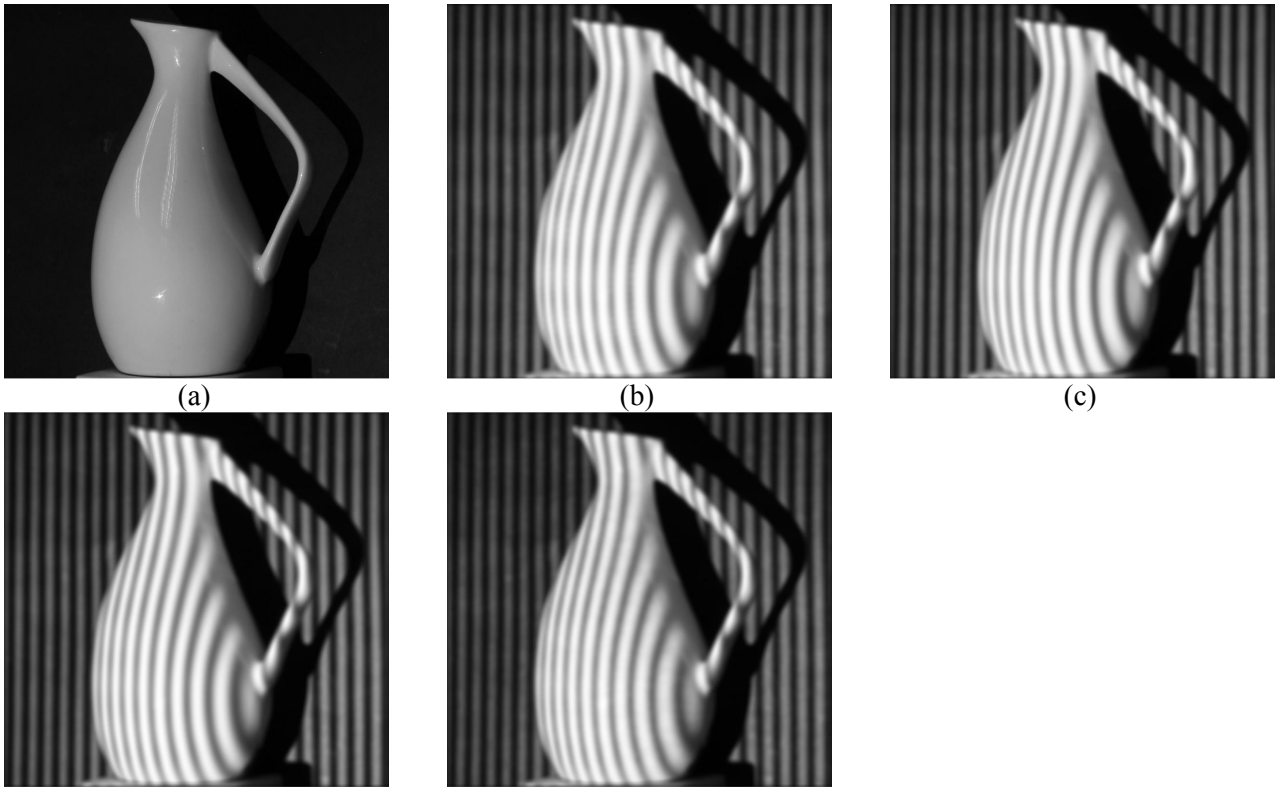

Fig. 8 Images captured when different fringe patterns are projected onto a measured object. (a) no projection, (b) *bptach*, (c) *cpatch*, (d) *cpatch1D* and (e) *cpatch2D*.

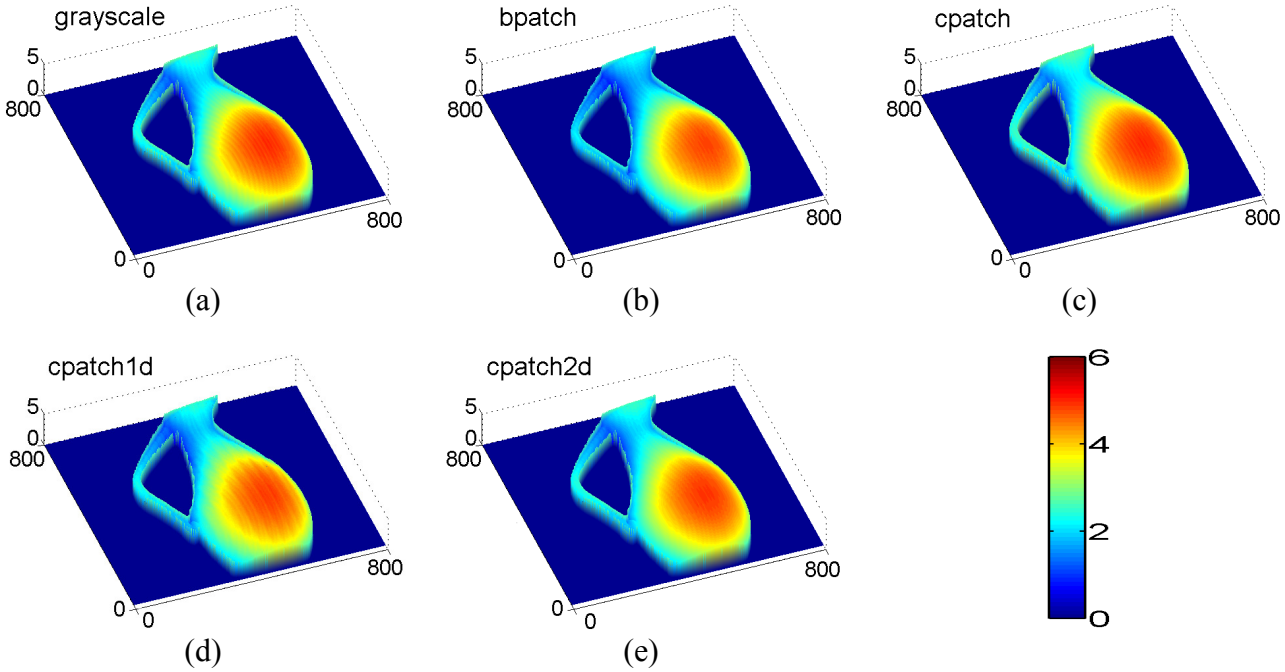

Fig. 9 Depth maps obtained with (a) sinusoidal fringe patterns, (b) *bptach*, (c) *cpatch*, (d) *cpatch1D* and (e) *cpatch2D*.